

pubs.acs.org/JPCL Letter

Efficient Charge Generation via Hole Transfer in Dilute Organic Donor-Fullerene Blends

Yin Song, Alexander Schubert, Xiao Liu, Srijana Bhandari, Stephen R. Forrest, Barry D. Dunietz, Eitan Geva, and Jennifer P. Ogilvie*



Cite This: J. Phys. Chem. Lett. 2020, 11, 2203–2210



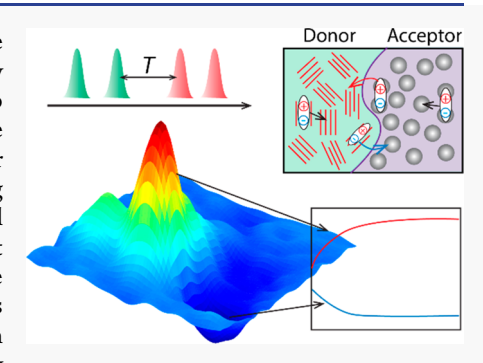
ACCESS

III Metrics & More

Article Recommendations

s Supporting Information

ABSTRACT: Efficient organic photovoltaics (OPVs) require broadband charge photogeneration with near-unity quantum yield. This can only be achieved by exploiting all pathways that generate charge. Electron transfer from organic donors to acceptors has been well-studied and is considered the primary path to charge photogeneration in OPVs. In contrast, much less is known about the hole transfer pathway. Here we study charge photogeneration in an archetypal system comprising tetraphenyldibenzoperiflanthene: C₇₀ blends using our recently developed multispectral two-dimensional electronic spectroscopy (M-2DES), supported by time-dependent density functional theory and fully quantum-mechanical Fermi's golden rule rate calculations. Our approach identifies in real time two rapid charge transfer pathways that are confirmed through computational analysis. Surprisingly, we find that both electron and hole transfer occur with comparable rates and efficiencies, facilitated by donor—acceptor electronic interactions. Our results highlight the importance of the



donor-acceptor electronic interactions. Our results highlight the importance of the hole transfer pathway for optimizing the efficiency of OPV devices employing small-molecule heterojunctions.

rganic photovoltaics (OPVs) commonly employ a donor:fullerene acceptor blend heterojunction (HJ) for light harvesting and charge generation. The charge generation process begins with absorption of a photon by either the donor or acceptor, forming an exciton. The exciton migrates to the donor-acceptor junction where the electron transfers to the acceptor or the hole to the donor. Hence, the charge transfer (CT) process is integral to photogeneration. To further improve the device efficiency, therefore, an understanding of the photophysical processes leading to CT is essential. ^{1–5} Due to the relatively low extinction coefficients of fullerenes in the solar spectral range, alternative CT pathways initiated by photoexcitation in the acceptor are often neglected. This concept has been challenged by several reports showing that low-donor-content devices (<10% weight ratio) can achieve similar or even higher-power-conversion efficiencies than higher-donor-content devices, 3,6-12 highlighting the importance of considering the mechanism of charge separation via the hole transfer pathway. Recently, several groups have reported the spectral dependence of charge generation yields when exciting the fullerene excitonic states in the ultraviolet and provided further evidence for the hole transfer pathway. $^{3,9-12}$ Armin and co-workers 10 have used a two-diode model to successfully describe the internal quantum efficiency in the visible range and propose that the hole transfer pathway is independent of excitation wavelength. Recent work on OPVs employing nonfullerene acceptors have highlighted the potential for exploiting the hole transfer pathway. 13-15 Furthermore, Kandada and co-workers have reported 16 that

electron transfer following energy transfer from fullerene to the donor can also contribute to charge generation. These findings await further verification and generalization to other OPV materials by real-time characterization techniques.

Here we combine multispectral two-dimensional electronic spectroscopy (M-2DES) with time-dependent density functional theory (TD-DFT) and rate theory to elucidate the mechanisms of charge transfer at donor-acceptor interfaces. 2DES has emerged as an effective tool to investigate photoexcitation dynamics in complex materials such as photosynthetic systems, 17-23 organic semiconducting materials, 24,25 and quantum dots. 26 Recently, it has been used to uncover mechanisms of electron transfer in conjugated polymer/fullerene blends, 24,25,27,28 although studies on hole transfer are still lacking. TD-DFT electronic structure calculations of dyad models have also been used to simulate complex interfacial processes in OPVs. 29-31 In this context. long-range interactions and polarization effects must be accounted for to achieve a reliable description of interfacial CT states.^{32–34} In this study, we employ an approach based on screened-range-separated hybrid functionals (SRSH) recently shown to accurately address condensed phase effects on

Received: January 7, 2020 Accepted: February 7, 2020 Published: February 7, 2020



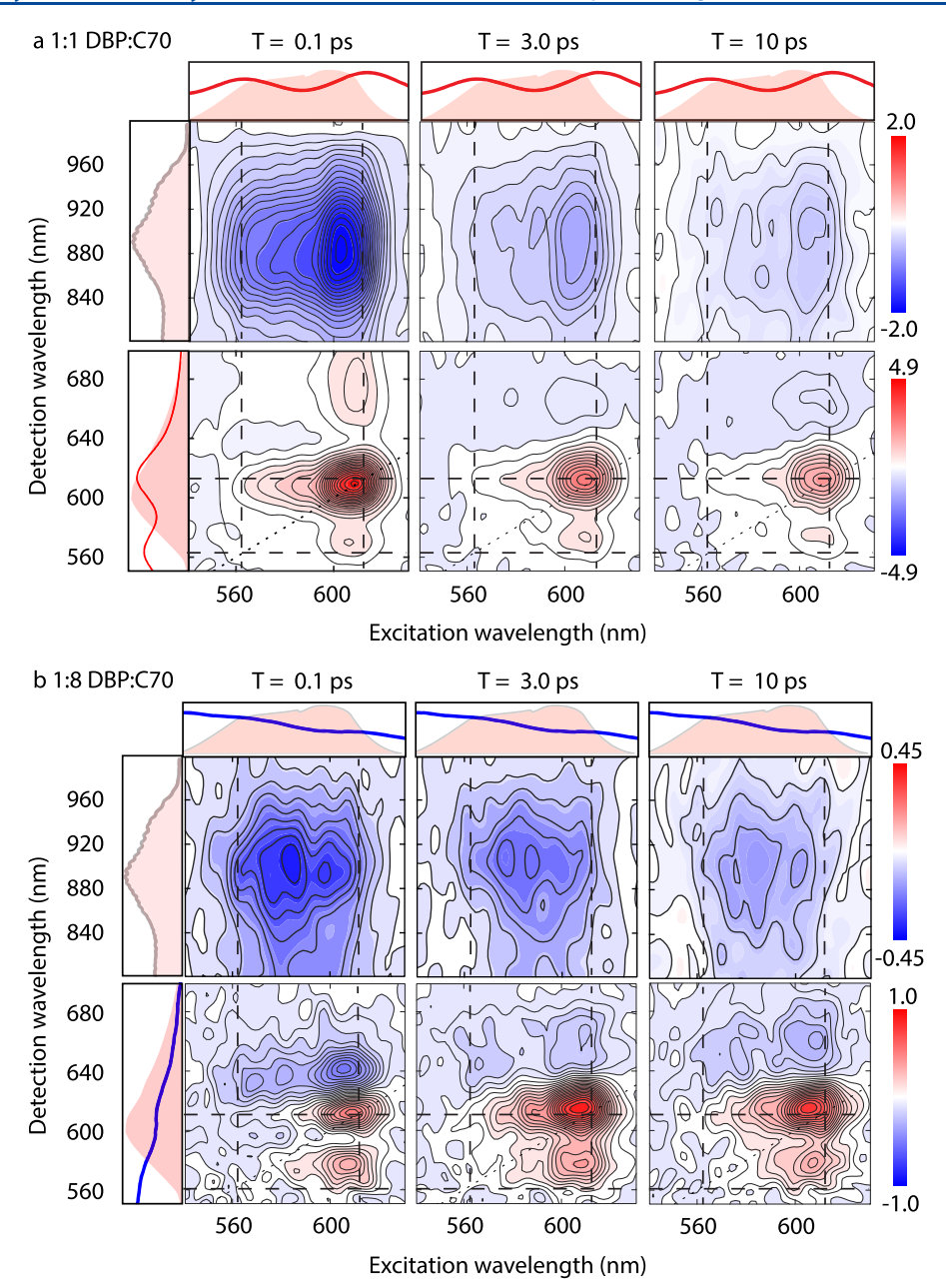


Figure 1. Absorptive 2DES of the DBP: C_{70} blends, alongside with the absorption, pump, and probe spectra. (a) 2DES of 1:1 DBP: C_{70} blend. Contour interval: 5% of the maximum amplitude. (b) 2DES of 1:8 DBP: C_{70} blend. Contour interval: 5% of the maximum amplitude in the visible 2DES and 10% of the maximum amplitude in near-IR 2DES. Dashed lines: 0–0 and 0–1 transitions of the DBP excitonic peaks. Blue solid lines to the left and on top of 2DES: absorption spectra of the DBP: C_{70} blends. Shaded pink: pump and probe spectra.

ground state transport properties³⁴ and excited state properties of solvated pigments.^{35,36} The polarization-consistent approach invokes SRSH within a polarizable continuum model (PCM) in TD-DFT calculations of the excited states. Electronic transition rate constants are then obtained following Fermi's golden rule^{29,37,38} based on the first-principles SRSH-PCM energy parameters. We apply this comprehensive approach to understand charge photogeneration in the archetypal donor—acceptor system comprising dilute tetraphenyldibenzoperiflanthene:fullerene (DBP:C₇₀) blends.⁶

Elucidating the kinetics of hole transfer in DBP: C_{70} blends is complicated by the overlapping absorption spectra of the constituents. The high-time and -frequency resolution of 2DES is ideally suited for resolving the spectral signatures of different processes that involve separate components of the bulk

heterojunction (BHJ) blend.^{39,40} More specifically, a 2D frequency spectrum is a map that correlates the photoexcited and the probed states. Compared with conventional pumpprobe spectroscopy, the additional excitation axis in 2DES enables direct monitoring of the kinetics of charge generation starting from different initial states. In 2DES, the photoexcited dynamics are encoded in the evolution of three signals: the ground state bleaching (GSB), stimulated emission (SE), and photoinduced absorption (PA). GSB is the nonlinear analog of linear absorption, revealing the loss of ground state molecules due to photoexcitation or energy or charge transfer. SE is analogous to fluorescence or phosphorescence of the excited molecules and appears at slightly longer wavelengths than GSB due to vibrational relaxation. PA reveals higher-lying absorptions from excited states including excitons, CT states,

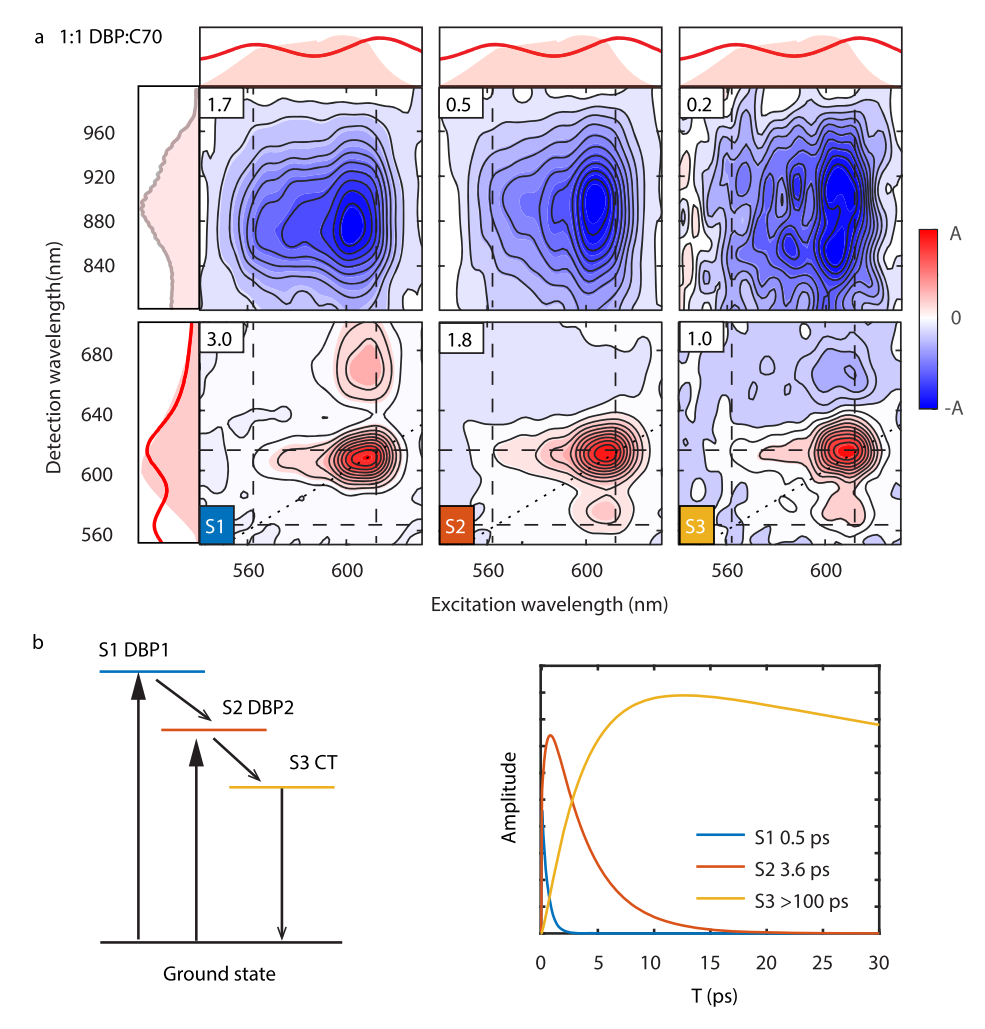


Figure 2. Global-target analysis of the 1:1 DBP: C_{70} blend. (a) Species-associated spectra of two DBP excitons (S1 and S2) and the CT product (S3). Contour interval: 10% of the maximum amplitude (A), which is displayed in the top-left corner of each plot. Dashed lines: 0–0 and 0–1 transitions of the DBP excitonic peaks. Red solid lines to the left and on top of 2DES: absorption spectra of the blend. Shaded pink: pump and probe spectra. (b) Kinetic model with two electron transfer pathways used in the analysis and the fitted time traces for two excitons and the CT product.

and polarons. A global analysis of the three signals is often required to establish a complete kinetic map of a particular dynamical process. One-color 2DES, which employs the same pump and probe pulses in the visible regime, has been used to investigate electron transfer in OPVs. ²⁴ However, it is desirable to extend the accessible frequency range from the visible to the near-infrared (IR) where PA signals of the organic donor and hole polarons are located. ^{41–43}

Here we apply multispectral 2DES (M-2DES) using both visible and near-IR probes to investigate charge transfer in the DBP: C_{70} blends. Figure 1a,b shows the respective absorptive M-2DES spectra of 1:1 and 1:8 DBP: C_{70} blend films at several different delays following excitation. At 0.1 ps, the 2D spectra of both blends exhibit a similar pattern of positive diagonal and cross peaks at \sim 610 and \sim 570 nm, which are attributed to GSB and SE signals associated with the dominant DBP transitions (i.e., $S_1^{\ \nu 0} \rightarrow S_0^{\ \nu 0}$ and $S_1^{\ \nu 1} \rightarrow S_0^{\ \nu 0}$, see Figure S1 and Sections S1 and S2). A negative signal is observed at 0.1 ps, at detection wavelengths spanning 800–1000 nm, and is assigned to PA of the DBP and C_{70} , consistent with pump–probe (Figure S2) and 2DES (Figure S3) measurements of neat films. These assignments are also consistent with our SRSH-PCM calculations (see Section S2 of SI). In the 1:1 DBP: C_{70}

blend, an additional SE corresponding to the $S_1^{\ \nu 0} \to S_0^{\ \nu 1}$ transition appears at $\lambda=660$ nm. This feature is absent in the 1:8 DBP: C_{70} blend, which instead shows a negative PA signal from $\lambda\approx625$ to 700 nm. This peak is attributed to PA of C_{70} , in accordance with previous studies⁴⁴ as well as our calculations (Table S1 and Section S2) and pump—probe measurements of C_{70} (Figure S2c).

After 3.0 ps, a negative-going feature from 640 to 690 nm arises in the 1:1 DBP:C₇₀ blend and lasts for >1 ns (see Figure S4 in SI). This feature is present at earlier times in the 1:8 DBP:C₇₀ blend. It is assigned to PA of the DBP hole polarons based on several observations: (1) The rise of PA from $\lambda = 640$ to 690 nm is only seen in blends, suggesting that this species is generated via charge transfer. (2) The GSB of DBP decays much slower than in a neat DBP film, which provides further evidence for the formation of a relatively long-lived CT species. (3) It has been reported that hole-polaron absorption in several conjugated molecules appears at the red edge of the absorption spectrum. 24,41,42 For example, P3HT films have an absorption peak at 604 nm and a hole polaron absorption band from 640 to 700 nm.^{24,41,42} Absorption of fullerene electron polarons has not been observed in this spectral range⁴⁴ and is not expected according to our computational analysis (see

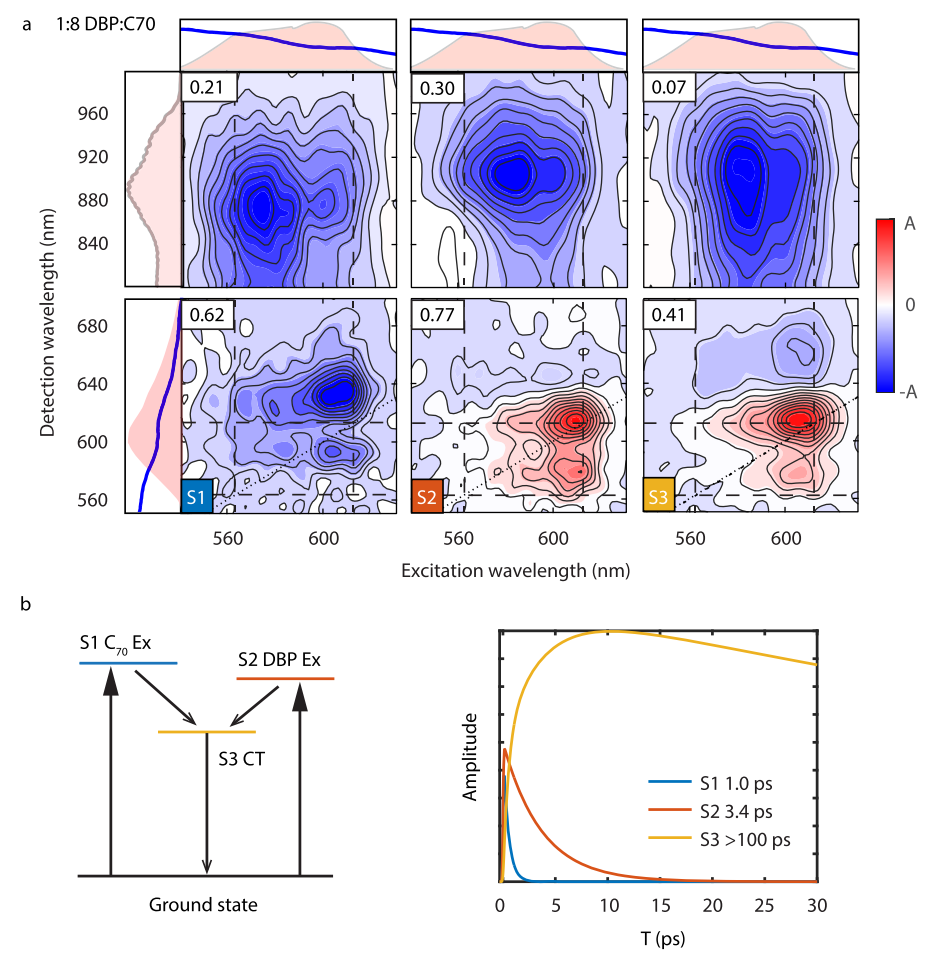


Figure 3. Global-target analysis of the 1:8 DBP: C_{70} blend. (a) Species-associated spectra of the C_{70} exciton (S1), DBP exciton (S2), and CT product (S3). Contour interval: 10% of the maximum amplitude (A), which is displayed in the top-left corner of each plot. Dashed lines: 0–0 and 0–1 transitions of the DBP excitonic peaks. Blue solid lines to the left and on top of 2DES: absorption spectra of the blend. (b) Kinetic model with an electron transfer and a hole transfer pathway and the fitted time traces for S1, S2, and S3.

Section S2 and Table S1 of the SI). It has been proposed that electroabsorption induced by the adjacent CT state or polarons can also appear on the red side of the donor absorption band. However, we exclude this possibility, since the transient absorption spectra of blends do not exhibit the characteristic first derivative line shape associated with electroabsorption, and broadening induced by the electric field of DBP is likely weak owing to its nonexistent dipole moment. In addition, we observe broad spectral band, long-lived PA from 800 to 1000 nm with a lifetime >1 ns in both 1:1 and 1:8 DBP:C₇₀ blends. We tentatively attribute this feature to absorption by CT states owing to the similar formation and decay rates with PA of the DBP hole polarons.

To quantitatively evaluate the charge generation pathways in the blends, we employ global-target analysis 47,48 of the M-2DES data, finding that three exponential terms are required to obtain a satisfactory fit for both samples. We tested possible models (see Figure S5 and Section S4 in the SI) and find that the model in Figures 2 and 3 provides a consistent picture for both blends. In the case of 1:1 DBP:C₇₀ (Figure 2), S1 represents excitons photogenerated inside the DBP domain that migrate to the DBP-C₇₀ interface with a time constant of 0.5 ± 0.2 ps. The aggregation of DBP into nanocrystalline domains and its impact on delocalized electronic states at the HJ interface have been investigated previously.^{7,49} Exciton S2,

located near the DBP– C_{70} interface, can be generated either by photoexcitation or energy transfer. It then dissociates into a CT state with a time constant of 3.6 \pm 0.2 ps. Species-associated spectra of both excitons are composed of GSB and PA of DBP, suggesting that the majority of photons are absorbed by DBP, as expected. The species-associated spectrum for S3 exhibits GSB of DBP and PA of the DBP hole polaron in the visible and CT state in the near-IR. This finding suggests that both DBP excitons transition into the same CT states.

Figure 3 shows global-target analysis results of the 1:8 DBP: C_{70} blend. In contrast to the 1:1 DBP: C_{70} blend, the S1 component exhibits very different spectral features as well as a longer lifetime $(1.0 \pm 0.1 \text{ ps})$. The species-associated spectrum for S1 is dominated by PA from $\lambda = 580$ to 680 nm, which resembles PA of the neat C_{70} film (see Figure S2c in the SI). We, therefore, attribute S1 to the C_{70} exciton, which is expected to be present in considerably higher concentration in the 1:8 DBP: C_{70} blend compared to the 1:1 DBP: C_{70} blend. We find that S2 has a similar spectral profile and lifetime to S2 in the 1:1 DBP: C_{70} blend, which we attribute to DBP excitons generated close to the heterointerface. Compared to the 1:1 blend, the 1:8 DBP: C_{70} blend contains a larger fraction of interfacial and considerably fewer bulk DBP molecules. Thus, the 1:8 DBP: C_{70} blends should exhibit predominantly

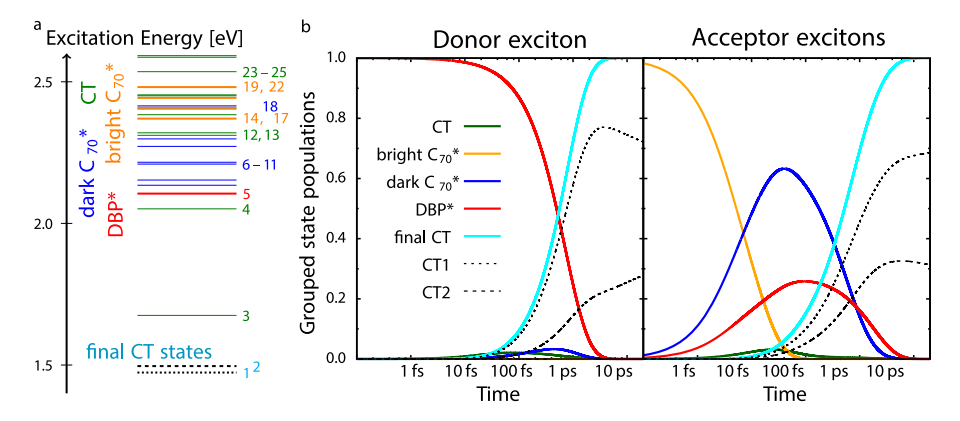


Figure 4. Interfacial excited electronic states of a dyad model and the simulated kinetics. (a) An energy-level diagram of 25 interfacial excited electronic states participating in the photoexcitation and the subsequent formation of two weakly coupled CT states. (b) Electron, hole, and exciton transfer kinetics based on the calculated Fermi's golden rule transition rates. Dotted and dashed black lines: simulated population dynamics revealing the formation of the two lowest CT states on similar time scales. Cyan curve: combined population dynamics of the two lowest CT states, which can be fit exponentially with time constants of 0.79 ps for donor excitons and 0.84 ps for acceptor excitons.

interfacial rather than bulk DBP excitons, indicating that our interpretation of the S2 exciton is consistent in blends with both high and low DBP concentrations. Interestingly, we find that both DBP and C_{70} excitons dissociate into common CT states whose spectral signatures appear in S3. Consistent with our analysis of the 1:1 DBP: C_{70} blend, S3 exhibits PA of the DBP hole polaron in the visible and of the CT states in the near-IR and has a similar lifetime. This finding suggests that there also exists an efficient charge generation pathway initiated by C_{70} photoexcitation, resulting in hole transfer into DBP.

Next, we turn to the computational analysis of the interfacial processes based on a DBP-C₇₀ dyad model. Previous studies have shown that CT states can be delocalized over both the DBP and C₇₀ domains and subsequently dissociate into chargeseparated states. Here, we focus on the early time dynamics following photoexcitation that involves multiple excited states. As energy and charge transfer processes strongly depend on the excitation energies, we employ the polarization-consistent SRSH-PCM framework, which has been shown to yield accurate excitation energies for both excited and CT states of condensed phase molecular systems. 34,36 Our analysis considers a DBP-C₇₀ complex in its optimized geometry, assuming that delocalization effects become relevant only on later time scales. Accounting for the spectral range of the pump laser (Figure S1a), 25 relevant electronic states have been identified as shown in Figure 4a, alongside the identification of the specific configurations. Within the interfacial model of the molecular complex, only a single excited DBP state (state 5) is found. We therefore interpret the occurrence of the second exciton in the 1:1 DBP: C_{70} blend, which is absent in the 1:8 DBP:C₇₀ blend, as due to delocalized excitons within the DBP domains. 7,49 A simulation of its fast transition (0.5 \pm 0.2 ps) into an interfacial DBP-exciton would require a trimolecular model that goes beyond the scope of this analysis.

Given the foregoing discussion, we restrict our analysis to the interfacial excited donor state (state 5, red). However, several $\rm C_{70}$ -excited states can be seen: four bright states with significant oscillator strengths are found (states 14, 17, 19, and 22, orange) as well as multiple dark states of low oscillator strength (6–11, 18, blue). CT states are found throughout the energy range (1–4, 12, 13, 15, 16, 20, 21, 23–25, green). Most notably, electronic densities of the four lowest CT states (1–4)

differ from each other only on the anionic C_{70} site and are, therefore, expected to share the same spectroscopic signature as the DBP hole–polaron PA signal. Further information about the states can be found in Table S2 of the SI.

To model the charge generation process, 600 transition rate constants between all 25 states were calculated based on Fermi's golden rule (see SI, Section S5 for further details). To this end, molecular reorganization energies were approximated by characteristic single-molecule deformations for the different transition types. A kinetic model was applied to simulate the population dynamics induced by either a donor or an acceptor exciton reaching the interface. The results are shown in Figure 4b, where the populations of states that share the same electronic properties, as indicated by color in Figure 4a, have been grouped for the sake of clarity. The donor exciton (Figure 4b, left panel, red curve) shows a transition via electron transfer into the two lowest CT states (cyan curve), whose DBP hole polaron PA signatures are indistinguishable due to the same electronic configuration on the DBP+ side. Furthermore, the combined population of both states is described by a single exponential rise with a time constant of 0.8 ps, corresponding to the single CT rate of an experimentally observed 3.6 \pm 0.2 ps (S2 to S3 in Figure 2). Considering the limitations of the dyad approach and the assumptions made within the Fermi's golden rule approach (e.g., the harmonic and perturbative approximations), we view a deviation within 1 order of magnitude to be in reasonable agreement.

A more complex picture is associated with C_{70} excitons. Immediately upon population of the four C_{70} -localized excited states (orange curve)—be it through photoexcitation or via excitons reaching the donor:acceptor interface—several transitions on the femtosecond time scale occur. These are not resolved experimentally due to their ultrashort lifetimes and the presence of coherent artifacts on this time scale. Two decay channels are dominant: (1) exciton transfer toward the energetically favored DBP site (red), and (2) intramolecular relaxation into lower-lying dark excited C_{70} states (blue). Both groups of states are transiently populated for approximately 1 ps. This indicates that efficient Förster resonant energy transfer (FRET) from bright C_{70} states (orange curves in Figure 4b, right panel) toward the DBP (red) occurs at the interface, which is suppressed for the dark C_{70} states (blue) due to their

vanishing transition dipole moments. The subsequent slower transitions populate the two lowest CT states (state 1 and 2, cyan). More specifically, they correspond to both electron transfer from the DBP-localized excited state (state 5) with an effective time constant of 1.8 ps (corresponding to S1 in the experiment: 3.4 \pm 0.2 ps), and hole transfer from the C₇₀localized excited states (6 and 7) with a time constant of 0.7 ps (S2 in the experiment: 1.0 ± 0.2 ps), which is of the same time scale as hole transport within the DBP domain as determined in previous studies. 50 Note that the effective electron transfer time appears to be larger than the direct electron transfer time (0.8 ps) from DBP to C_{70} due to the repopulation of the DBP excited state from higher-lying excited states. Overall, we find that both pathways, originating in photoexcitation of either the donor or the acceptor, contribute with approximately equal efficiency to the charge generation process.

Ultrafast electron transfer in organic donor/acceptor blends has been reported in previous studies, $^{1,24,43,51-54}$ with the time scale ranging from hundreds of femtoseconds to tens of picoseconds. In the 1:1 DBP:C₇₀ blend, we find that excitons—either photoexcited within the DBP domain or at the donor—acceptor interface—transition into CT states within 3.4 ± 0.2 ps. This finding is further verified by computational analysis based on SRSH-PCM electronic structure calculations and Fermi's golden-rule-based transition rate constants. A similar electron transfer process has also been observed in the 1:8 DBP:C₇₀ blend. As both types of DBP excitons can be efficiently converted into common CT states, we conclude that energy loss is limited by charge separation and recombination but not by inefficient exciton diffusion to the donor/acceptor interface or the initial CT step.

Previous studies have shown that hole transfer is an important pathway for charge generation in the ultraviolet where the sunlight is predominantly absorbed by full-erenes. $^{3,9-12}$ In the 1:8 DBP:C₇₀ blend, we find evidence for a hole transfer pathway following the photoexcitation of C₇₀ in the visible, which is nearly as likely as electron transfer. This finding is consistent with the two-diode model that proposes that the hole transfer pathway is independent of excitation wavelength. 10 We note that Kandada and co-workers reported that charge generation originating from the PCBM exciton is via electron transfer following energy transfer from PCBM to P3HT. 16 Our calculations show that such exciton transfer from bright excited C₇₀ states competes with intramolecular relaxation to low-lying dark excited C70 states that cannot undergo further Förster energy transfer. However, our experiments show no evidence of such energy transfer. This may be rooted in its predicted fast time scale (<0.1 ps), which is inaccessible due to pulse-overlap artifacts,⁵⁵ and its spectral signatures might be masked by the photogenerated DBP

In summary, systematic analysis of charge transfer in DBP: C_{70} blends provides insight into the charge generation mechanisms in this archetypal OPV system. 2DES studies supported by Fermi's golden rule calculations of transition rates based on energies obtained using the SRSH-PCM framework reveal that the hole transfer from the acceptor significantly contributes to the high power-conversion efficiency in the low-donor-content (1:8 DBP: C_{70}) blend. The fast, 1 ps hole transfer rate indicates that no exciton diffusion occurs prior to hole transfer. Previous X-ray diffraction and transmission electron microscopy measurements show that C_{70} crystalline domains have a size of ~ 5 nm.

These findings imply that C_{70} excitons are delocalized over the crystalline domain. Such delocalization can facilitate hole transfer and subsequent charge separation. Another interesting finding is that the CT states are formed at similar rates via both the electron transfer and the hole transfer pathways. These CT states then dissociate into free charge carriers or recombine to the ground state. Our results underscore the importance of considering both electron and hole transfer pathways in the design of next generation OPV devices that minimize energy loss.

ASSOCIATED CONTENT

Supporting Information

The Supporting Information is available free of charge at https://pubs.acs.org/doi/10.1021/acs.jpclett.0c00058.

Linear absorption, photoluminescence, and spectral analysis; excitation energies based on TD-DFT calculations; ultrafast spectroscopic measurements of neat DBP film, neat C_{70} film and the DBP: C_{70} blends; justification of kinetic models used in global-target analysis; Fermi's golden rule transition rate constants; experimental and computational methods (PDF)

AUTHOR INFORMATION

Corresponding Author

Jennifer P. Ogilvie — Department of Physics, University of Michigan, Ann Arbor, Michigan 48109, United States; orcid.org/0000-0003-4060-5437; Email: jogilvie@umich.edu

Authors

Yin Song — Department of Physics, University of Michigan, Ann Arbor, Michigan 48109, United States; orcid.org/0000-0001-8978-2958

Alexander Schubert — Department of Chemistry, University of Michigan, Ann Arbor, Michigan 48109, United States; Department of Chemistry and Biochemistry, Kent State University, Kent, Ohio 44242, United States; orcid.org/0000-0002-8560-6436

Xiao Liu – Department of Electrical Engineering and Computer Science, University of Michigan, Ann Arbor, Michigan 48109, United States; Oorcid.org/0000-0002-5397-6694

Srijana Bhandari – Department of Chemistry and Biochemistry, Kent State University, Kent, Ohio 44242, United States

Stephen R. Forrest — Department of Physics, Department of Electrical Engineering and Computer Science, and Department of Material Science and Engineering, University of Michigan, Ann Arbor, Michigan 48109, United States; orcid.org/0000-0003-0131-1903

Barry D. Dunietz – Department of Chemistry and Biochemistry, Kent State University, Kent, Ohio 44242, United States;
orcid.org/0000-0002-6982-8995

Eitan Geva — Department of Chemistry, University of Michigan, Ann Arbor, Michigan 48109, United States; orcid.org/ 0000-0002-7935-4586

Complete contact information is available at: https://pubs.acs.org/10.1021/acs.jpclett.0c00058

Notes

The authors declare no competing financial interest.

ACKNOWLEDGMENTS

Y.S., S.R.F., and J.P.O. acknowledge the support of the National Science Foundation through instrumentation grant #CHE-1428479 and grant #DMR-1905401. Y.S. acknowledges the support of the Natural Sciences and Engineering Council of Canada (NSERC) for a Postdoctoral Fellowship. A.S. is grateful for support by an Institute for Complex Adaptive Matter (ICAM) fellowship, awarded by Kent State University and University of Michigan ICAM branches. B.D.D. is grateful for support by NSF Grant CHE-1362504. E.G. is grateful for support by the NSF via Grants CHE-1464477 and CHE-1800325. B.D.D. and E.G. are grateful for support by DOE Grant DE-SC0016501. S.R.F. acknowledges the support of the U.S. Department of Energy, Office of Science, Basic Energy Sciences, under Award #DE-SC0017971. J.P.O., E.G., and S.R.F. gratefully acknowledge funding through the Mcubed Program by the University of Michigan. Y.S. thanks Mikas Vengris for assistance with the CarpetView software. Y.S. thanks Ryan D. Pensack for insightful discussion and comments on the manuscript.

REFERENCES

- (1) Clarke, T. M.; Durrant, J. R. Charge Photogeneration in Organic Solar Cells. *Chem. Rev.* **2010**, *110* (11), 6736–6767.
- (2) Few, S.; Frost, J. M.; Nelson, J. Models of charge pair generation in organic solar cells. *Phys. Chem. Chem. Phys.* **2015**, 17 (4), 2311–2325
- (3) Stoltzfus, D. M.; Donaghey, J. E.; Armin, A.; Shaw, P. E.; Burn, P. L.; Meredith, P. Charge Generation Pathways in Organic Solar Cells: Assessing the Contribution from the Electron Acceptor. *Chem. Rev.* **2016**, *116* (21), 12920–12955.
- (4) Reid, O. G.; Pensack, R. D.; Song, Y.; Scholes, G. D.; Rumbles, G. Charge Photogeneration in Neat Conjugated Polymers. *Chem. Mater.* **2014**, 26 (1), 561–575.
- (5) Ponseca, C. S.; Chabera, P.; Uhlig, J.; Persson, P.; Sundstrom, V. Ultrafast Electron Dynamics in Solar Energy Conversion. *Chem. Rev.* **2017**, *117* (16), 10940–11024.
- (6) Xiao, X.; Zimmerman, J. D.; Lassiter, B. E.; Bergemann, K. J.; Forrest, S. R. A hybrid planar-mixed tetraphenyldibenzoperiflanthene/C70 photovoltaic cell. *Appl. Phys. Lett.* **2013**, *102* (7), 073302.
- (7) Liu, X.; Ding, K.; Panda, A.; Forrest, S. R. Charge Transfer States in Dilute Donor–Acceptor Blend Organic Heterojunctions. *ACS Nano* **2016**, *10* (8), 7619–7626.
- (8) Xiao, X.; Bergemann, K. J.; Zimmerman, J. D.; Lee, K.; Forrest, S. R. Small-Molecule Planar-Mixed Heterojunction Photovoltaic Cells with Fullerene-Based Electron Filtering Buffers. *Adv. Energy Mater.* **2014**, *4* (7), 1301557.
- (9) Bakulin, A. A.; Dimitrov, S. D.; Rao, A.; Chow, P. C. Y.; Nielsen, C. B.; Schroeder, B. C.; McCulloch, I.; Bakker, H. J.; Durrant, J. R.; Friend, R. H. Charge-Transfer State Dynamics Following Hole and Electron Transfer in Organic Photovoltaic Devices. *J. Phys. Chem. Lett.* **2013**, *4* (1), 209–215.
- (10) Armin, A.; Kassal, I.; Shaw, P. E.; Hambsch, M.; Stolterfoht, M.; Lyons, D. M.; Li, J.; Shi, Z.; Burn, P. L.; Meredith, P. Spectral Dependence of the Internal Quantum Efficiency of Organic Solar Cells: Effect of Charge Generation Pathways. *J. Am. Chem. Soc.* **2014**, 136 (32), 11465–11472.
- (11) Kozlov, O. V.; Pavelyev, V. G.; de Gier, H. D.; Havenith, R. W. A.; van Loosdrecht, P. H.M.; Hummelen, J. C.; Pshenichnikov, M. S. Ultrafast electron and hole transfer in bulk heterojunctions of low-bandgap polymers. *Organic Photonics and Photovoltaics* **2016**, *4*, 24–34.
- (12) Hendriks, K. H.; Wijpkema, A. S. G.; van Franeker, J. J.; Wienk, M. M.; Janssen, R. A. J. Dichotomous Role of Exciting the Donor or the Acceptor on Charge Generation in Organic Solar Cells. *J. Am. Chem. Soc.* **2016**, *138* (31), 10026–10031.

- (13) Zhang, G.; Zhao, J.; Chow, P. C. Y.; Jiang, K.; Zhang, J.; Zhu, Z.; Zhang, J.; Huang, F.; Yan, H. Nonfullerene Acceptor Molecules for Bulk Heterojunction Organic Solar Cells. *Chem. Rev.* **2018**, *118* (7), 3447–3507.
- (14) Chen, S.; Wang, Y.; Zhang, L.; Zhao, J.; Chen, Y.; Zhu, D.; Yao, H.; Zhang, G.; Ma, W.; Friend, R. H.; Chow, P. C. Y.; Gao, F.; Yan, H. Efficient Nonfullerene Organic Solar Cells with Small Driving Forces for Both Hole and Electron Transfer. *Adv. Mater.* **2018**, *30* (45), 1804215.
- (15) Douglas, J. D.; Chen, M. S.; Niskala, J. R.; Lee, O. P.; Yiu, A. T.; Young, E. P.; Fréchet, J. M. J. Solution-Processed, Molecular Photovoltaics that Exploit Hole Transfer from Non-Fullerene, n-Type Materials. *Adv. Mater.* **2014**, *26* (25), 4313–4319.
- (16) Kandada, A. R.; Grancini, G.; Petrozza, A.; Perissinotto, S.; Fazzi, D.; Raavi, S. S.; Lanzani, G. Ultrafast energy transfer in ultrathin organic donor/acceptor blend. *Sci. Rep.* **2013**, *3*, 2073.
- (17) Brixner, T.; Stenger, J.; Vaswani, H. M.; Cho, M.; Blankenship, R. E.; Fleming, G. R. Two-dimensional spectroscopy of electronic couplings in photosynthesis. *Nature* **2005**, 434 (7033), 625–628.
- (18) Engel, G. S.; Calhoun, T. R.; Read, E. L.; Ahn, T. K.; Mancal, T.; Cheng, Y. C.; Blankenship, R. E.; Fleming, G. R. Evidence for wavelike energy transfer through quantum coherence in photosynthetic systems. *Nature* **2007**, *446* (7137), 782–6.
- (19) Collini, E.; Wong, C. Y.; Wilk, K. E.; Curmi, P. M.; Brumer, P.; Scholes, G. D. Coherently wired light-harvesting in photosynthetic marine algae at ambient temperature. *Nature* **2010**, *463* (7281), 644–7
- (20) Fuller, F. D.; Pan, J.; Gelzinis, A.; Butkus, V.; Senlik, S. S.; Wilcox, D. E.; Yocum, C. F.; Valkunas, L.; Abramavicius, D.; Ogilvie, J. P. Vibronic coherence in oxygenic photosynthesis. *Nat. Chem.* **2014**, 6 (8), 706–711.
- (21) Ostroumov, E. E.; Mulvaney, R. M.; Cogdell, R. J.; Scholes, G. D. Broadband 2D Electronic Spectroscopy Reveals a Carotenoid Dark State in Purple Bacteria. *Science* **2013**, *340* (6128), 52–56.
- (22) Duan, H. G.; Prokhorenko, V. I.; Cogdell, R. J.; Ashraf, K.; Stevens, A. L.; Thorwart, M.; Miller, R. J. D. Nature does not rely on long-lived electronic quantum coherence for photosynthetic energy transfer. *Proc. Natl. Acad. Sci. U. S. A.* **2017**, *114* (32), 8493–8498.
- (23) Romero, E.; Augulis, R.; Novoderezhkin, V. I.; Ferretti, M.; Thieme, J.; Zigmantas, D.; van Grondelle, R. Quantum coherence in photosynthesis for efficient solar-energy conversion. *Nat. Phys.* **2014**, 10 (9), 676.
- (24) Song, Y.; Clafton, S. N.; Pensack, R. D.; Kee, T. W.; Scholes, G. D. Vibrational coherence probes the mechanism of ultrafast electron transfer in polymer-fullerene blends. *Nat. Commun.* **2014**, *5* (1), 4933.
- (25) De Sio, A.; Troiani, F.; Maiuri, M.; Rehault, J.; Sommer, E.; Lim, J.; Huelga, S. F.; Plenio, M. B.; Rozzi, C. A.; Cerullo, G.; Molinari, E.; Lienau, C. Tracking the coherent generation of polaron pairs in conjugated polymers. *Nat. Commun.* **2016**, *7* (1), 13742.
- (26) Stone, K. W.; Turner, D. B.; Gundogdu, K.; Cundiff, S. T.; Nelson, K. A. Exciton-Exciton Correlations Revealed by Two-Quantum, Two-Dimensional Fourier Transform Optical Spectroscopy. *Acc. Chem. Res.* **2009**, 42 (9), 1452–1461.
- (27) Song, Y.; Hellmann, C.; Stingelin, N.; Scholes, G. D. The separation of vibrational coherence from ground- and excited-electronic states in P3HT film. *J. Chem. Phys.* **2015**, 142 (21), 212410.
- (28) Collini, E.; Scholes, G. D. Coherent Intrachain Energy Migration in a Conjugated Polymer at Room Temperature. *Science* **2009**, 323 (5912), 369–373.
- (29) Lee, M. H.; Geva, E.; Dunietz, B. D. Calculation from First-Principles of Golden Rule Rate Constants for Photoinduced Subphthalocyanine/Fullerene Interfacial Charge Transfer and Recombination in Organic Photovoltaic Cells. *J. Phys. Chem. C* **2014**, *118* (18), 9780–9789.
- (30) Wilcox, D. E.; Lee, M. H.; Sykes, M. E.; Niedringhaus, A.; Geva, E.; Dunietz, B. D.; Shtein, M.; Ogilvie, J. P. Ultrafast Charge-Transfer Dynamics at the Boron Subphthalocyanine Chloride/C60 Heterojunction: Comparison between Experiment and Theory. *J. Phys. Chem. Lett.* **2015**, *6* (3), 569–575.

- (31) Lee, M. H.; Dunietz, B. D.; Geva, E. Donor-to-Donor vs Donor-to-Acceptor Interfacial Charge Transfer States in the Phthalocyanine-Fullerene Organic Photovoltaic System. *J. Phys. Chem. Lett.* **2014**, *5* (21), 3810–3816.
- (32) Zheng, Z.; Egger, D. A.; Brédas, J.-L.; Kronik, L.; Coropceanu, V. Effect of Solid-State Polarization on Charge-Transfer Excitations and Transport Levels at Organic Interfaces from a Screened Range-Separated Hybrid Functional. *J. Phys. Chem. Lett.* **2017**, 8 (14), 3277—3283.
- (33) Kronik, L.; Kümmel, S. Dielectric Screening Meets Optimally Tuned Density Functionals. *Adv. Mater.* **2018**, *30* (41), 1706560.
- (34) Bhandari, S.; Cheung, M. S.; Geva, E.; Kronik, L.; Dunietz, B. D. Fundamental Gaps of Condensed-Phase Organic Semiconductors from Single-Molecule Calculations using Polarization-Consistent Optimally Tuned Screened Range-Separated Hybrid Functionals. *J. Chem. Theory Comput.* **2018**, *14* (12), 6287–6294.
- (35) Song, Y.; Schubert, A.; Maret, E.; Burdick, R. K.; Dunietz, B.; Geva, E.; Ogilvie, J. Vibronic structure of photosynthetic pigments probed by polarized two-dimensional electronic spectroscopy and ab initio calculations. *Chemical Science* **2019**, *10* (10), 8143–8153.
- (36) Bhandari, S.; Dunietz, B. D. Quantitative Accuracy in Calculating Charge Transfer State Energies in Solvated Molecular Complexes Using a Screened Range Separated Hybrid Functional within a Polarized Continuum Model. *J. Chem. Theory Comput.* **2019**, *15* (8), 4305–4311.
- (37) Sun, X.; Geva, E. Equilibrium Fermi's Golden Rule Charge Transfer Rate Constants in the Condensed Phase: The Linearized Semiclassical Method vs Classical Marcus Theory. *J. Phys. Chem. A* **2016**, 120 (19), 2976–2990.
- (38) Aksu, H.; Schubert, A.; Geva, E.; Dunietz, B. D. Explaining Spectral Asymmetries and Excitonic Characters of the Core Pigment Pairs in the Bacterial Reaction Center Using a Screened Range-Separated Hybrid Functional. *J. Phys. Chem. B* **2019**, *123* (42), 8970–8975.
- (39) Anna, J. M.; Song, Y.; Dinshaw, R.; Scholes, G. D. Two-dimensional electronic spectroscopy for mapping molecular photophysics. *Pure Appl. Chem.* **2013**, *85* (7), 1307–1319.
- (40) Song, Y.; Konar, A.; Sechrist, R.; Roy, V. P.; Duan, R.; Dziurgot, J.; Policht, V.; Matutes, Y. A.; Kubarych, K. J.; Ogilvie, J. P. Multispectral multidimensional spectrometer spanning the ultraviolet to the mid-infrared. *Rev. Sci. Instrum.* **2019**, *90* (1), 013108.
- (41) Guo, J. M.; Ohkita, H.; Benten, H.; Ito, S. Charge Generation and Recombination Dynamics in Poly(3-hexylthiophene)/Fullerene Blend Films with Different Regioregularities and Morphologies. *J. Am. Chem. Soc.* **2010**, *132* (17), 6154–6164.
- (42) Osterbacka, R.; An, C. P.; Jiang, X. M.; Vardeny, Z. V. Two-dimensional electronic excitations in self-assembled conjugated polymer nanocrystals. *Science* **2000**, 287 (5454), 839–842.
- (43) Grancini, G.; Maiuri, M.; Fazzi, D.; Petrozza, A.; Egelhaaf, H. J.; Brida, D.; Cerullo, G.; Lanzani, G. Hot exciton dissociation in polymer solar cells. *Nat. Mater.* **2013**, *12* (1), 29–33.
- (44) Causa, M.; Ramirez, I.; Martinez Hardigree, J. F.; Riede, M.; Banerji, N. Femtosecond Dynamics of Photoexcited C60 Films. *J. Phys. Chem. Lett.* **2018**, *9* (8), 1885–1892.
- (45) Tamai, Y.; Fan, Y.; Kim, V. O.; Ziabrev, K.; Rao, A.; Barlow, S.; Marder, S. R.; Friend, R. H.; Menke, S. M. Ultrafast Long-Range Charge Separation in Nonfullerene Organic Solar Cells. *ACS Nano* **2017**, *11* (12), 12473–12481.
- (46) Gelinas, S.; Rao, A.; Kumar, A.; Smith, S. L.; Chin, A. W.; Clark, J.; van der Poll, T. S.; Bazan, G. C.; Friend, R. H. Ultrafast Long-Range Charge Separation in Organic Semiconductor Photovoltaic Diodes. *Science* **2014**, 343 (6170), 512–516.
- (47) van Stokkum, I. H. M.; Larsen, D. S.; van Grondelle, R. Global and target analysis of time-resolved spectra. *Biochim. Biophys. Acta, Bioenerg.* **2004**, *1657* (2), 82–104.
- (48) Holzwarth, A. R. Data Analysis of Time-Resolved Measurements. *Biophysical Techniques in Photosynthesis* **1996**, 3, 75–92.

- (49) Ding, K.; Liu, X.; Forrest, S. R. Charge Transfer and Collection in Dilute Organic Donor–Acceptor Heterojunction Blends. *Nano Lett.* **2018**, *18* (5), 3180–3184.
- (50) Griffith, O. L.; Liu, X.; Amonoo, J. A.; Djurovich, P. I.; Thompson, M. E.; Green, P. F.; Forrest, S. R. Charge transport and exciton dissociation in organic solar cells consisting of dipolar donors mixed with C70. *Phys. Rev. B: Condens. Matter Mater. Phys.* **2015**, 92 (8), 085404.
- (51) Jakowetz, A. C.; Bohm, M. L.; Zhang, J.; Sadhanala, A.; Huettner, S.; Bakulin, A. A.; Rao, A.; Friend, R. H. What Controls the Rate of Ultrafast Charge Transfer and Charge Separation Efficiency in Organic Photovoltaic Blends. J. Am. Chem. Soc. 2016, 138 (36), 11672–9.
- (52) Cook, S.; Katoh, R.; Furube, A. Ultrafast Studies of Charge Generation in PCBM:P3HT Blend Films following Excitation of the Fullerene PCBM. *J. Phys. Chem. C* **2009**, *113* (6), 2547–2552.
- (53) Pensack, R. D.; Banyas, K. M.; Barbour, L. W.; Hegadorn, M.; Asbury, J. B. Ultrafast vibrational spectroscopy of charge-carrier dynamics in organic photovoltaic materials. *Phys. Chem. Chem. Phys.* **2009**, *11* (15), 2575–91.
- (54) Tamura, H.; Burghardt, I. Ultrafast Charge Separation in Organic Photovoltaics Enhanced by Charge Delocalization and Vibronically Hot Exciton Dissociation. *J. Am. Chem. Soc.* **2013**, *135* (44), 16364–16367.
- (55) Kovalenko, S. A.; Dobryakov, A. L.; Ruthmann, J.; Ernsting, N. P. Femtosecond spectroscopy of condensed phases with chirped supercontinuum probing. *Phys. Rev. A: At., Mol., Opt. Phys.* **1999**, 59 (3), 2369–2384.